Effects of annealing temperatures on the morphological, mechanical, surface chemical bonding, and solar selectivity properties of sputtered TiAlSiN thin films

Rahman, M. Mahbubur; Jiang, Zhong-tao; Zhou, Zhi-feng; Xie, Zonghan; Yin, Chun Yang; Kabir, Humayun; Haque, Md. Mahbubul; Amri, Amun; Mondinos, Nicholas; Altarawneh, Mohammednoor

DOI:
10.1016/j.jallcom.2016.02.077

Accepted Manuscript

Effects of annealing temperatures on the morphological, mechanical, surface chemical bonding, and solar selectivity properties of sputtered TiAlSiN thin films

M. Mahbubur Rahman, Zhong-Tao Jiang, Zhi-feng Zhou, Zonghan Xie, Chun Yang Yin, Humayun Kabir, Md. Mahbubul Haque, Amun Amri, Nicholas Mondinos, Mohammednoor Altarawneh

PII: S0925-8388(16)30346-2

DOI: 10.1016/j.jallcom.2016.02.077

Reference: JALCOM 36688

To appear in: *Journal of Alloys and Compounds*

Received Date: 21 December 2015

Revised Date: 5 February 2016

Accepted Date: 8 February 2016

Please cite this article as: M.M. Rahman, Z.-T. Jiang, Z.-f. Zhou, Z. Xie, C.Y. Yin, H. Kabir, M.M. Haque, A. Amri, N. Mondinos, M. Altarawneh, Effects of annealing temperatures on the morphological, mechanical, surface chemical bonding, and solar selectivity properties of sputtered TiAlSiN thin films, *Journal of Alloys and Compounds* (2016), doi: 10.1016/j.jallcom.2016.02.077.

Effects of annealing temperatures on the morphological, mechanical, surface chemical bonding, and solar selectivity properties of sputtered TiAlSiN thin films

M. Mahbubur Rahman[1*], Zhong-Tao Jiang[1*], Zhi-feng Zhou[2], Zonghan Xie[3], Chun Yang Yin[4], Humayun Kabir[5], Md. Mahbubul Haque[6], Amun Amri[7], Nicholas Mondinos[1], Mohammednoor Altarawneh[8]

[1] Surface Analysis and Materials Engineering Research Group
School of Engineering & Information Technology, Murdoch University, Murdoch, Western Australia 6150, Australia

[2]Department of Mechanical and Biomedical Engineering, City University of Hong Kong, Kowloon, Hong Kong, China

[3]School of Mechanical Engineering, University of Adelaide, SA 5005, Australia

[4]School of Science and Engineering, Teesside University, Borough Road, Middlesbrough, TS1 3BA, United Kingdom

[5]School of Metallurgy and Materials, University of Birmingham, Edgbaston, Birmingham B15 2TT, United Kingdom

[6]Materials Science Division, Atomic Energy Centre Dhaka, Dhaka 1000, Bangladesh

[7]Department of Chemical Engineering, Riau University, Pekanbaru, Indonesia

[8]School of Engineering & Information Technology, Murdoch University, Murdoch, Western Australia 6150, Australia

[*]Corresponding Authors: M.Rahman@Murdoch.edu.au (M.M. Rahman)
Z.Jiang@Murdoch.edu.au (Z.-T. Jiang)

ABSTRACT

Quaternary sputtered TiAlSiN coatings were investigated for their high temperature structural stability, surface morphology, mechanical behaviors, surface chemical bonding states, solar absorptance and thermal emittance for possible solar selective surface applications. The TiAlSiN films were synthesized, via unbalanced magnetron sputtered technology, on AISI M2 steel substrate and annealed at 500 °C - 800 °C temperature range. SEM micrographs show nanocomposite-like structure with amorphous grain boundaries. Nanoindentation analyses

indicate a decrease of hardness, plastic deformation and constant yield strength for the coatings. XPS analysis show mixed Ti, Al and Si nitride and oxide as main coating components but at 800 °C the top layer of the coatings is clearly composed of only Ti and Al oxides. Synchrotron radiation XRD (SR-XRD) results indicate various Ti, Al and Si nitride and oxide phases, for the above annealing temperature range with a phase change occurring with the Fe component of the substrate. UV-Vis spectroscopy, FTIR spectroscopy studies determined a high solar selectivity, *s* of 24.6 for the sample annealed at 600 °C. Overall results show good structural and morphological stability of these coatings at temperatures up to 800 °C with a very good solar selectivity for real world applications.

Keywords: magnetron sputtering; thin film coatings; optical properties; solar absorptance; solar emittance; selective solar surface.

1. Introduction

Transition metal nitride based quaternary TiAlSiN coatings are attractive candidates as cutting tools, protective and decorative coatings due to their many outstanding properties [1]. In recent years they have seen significant interest as solar selective absorbers for harvesting solar energy in various applications such as thermal solar collectors, solar steam generators and steam turbines for producing the electricity at mid and mid-to high temperatures [2-13]. A good selective surface must have high absorptance (α) in the visible spectrum up to 2.5 µm and low emittance (ε) in the infra-red (IR) region $\geq$ 2.5 µm at the operating temperatures. In recent years, transition metal nitride based tandem coatings (e.g., TiAlN/AlON, and TiAl/TiAlN/TiAlON/TiAlO) have been suggested for use in solar selective surfaces to be used in photothermal applications [4, 14]. Barshilia et al. [15] developed a high thermal stable TiAlN/TiAlON/Si_3N_4 tandem absorber on a copper substrate for high temperature solar selective applications that exhibited an absorptance of 0.958 and an emittance of 0.07. Until now these materials have not been commercially produced [4, 11, 16]. Transition metal oxides based thin film coatings with good optical properties have been also developed for solar selective surface applications [17-22].

Most of the solar selective coatings exhibit good stability in a vacuum but in air they have very limited thermal stability. However, in a high temperature or for long period application purposes, these solar selective absorbers should have stable structural configuration minimal degradations. The oxidation resistance behaviour of these coatings is also very important as they are frequently exposed at high temperature atmospheres in air.

The addition of Al and Si to the TiN coatings increases their oxidation resistance by forming oxide layers around the surface which eventually work as a barrier for further oxygen penetrations at high temperatures. The formation of amorphous phases also provides better stability against degradation, corrosion and oxidation than that of crystalline metallic nitride phases. TiAlSiN coatings provide good thermal stability at temperatures above 800 °C [26, 27]. These coatings have been explored mostly for their extraordinary mechanical properties, but as applications in solar selective surfaces in thermal collector devices are relatively unexplored [28-31].

The synchrotron radiation X-ray diffraction (SR-XRD technique is successfully used to probe the crystalline and electronic structure of various systems in a wide range of fields such as physics, chemistry, environmental sciences, materials sciences, biology, medicine, and geophysics. The SR-XRD offers many advantages over the conventional laboratory based XRD techniques such as: highly collimated and intense photon beams, photon-energy tune ability, exceptional photon wavelength resolution ($\Delta\lambda/\lambda \approx 2 \times 10^{-4}$), polarization control, coherence, very high signal-to-noise and signal-to-background ratio. The synchrotron techniques are extensively used in the identification of phases in compounds and unknown structural forms developed during the synthesis processes of the films. In recent years these techniques successfully investigated the local electronic structure of metal nitride thin films in pure and doped states [23-25].

To the best of our knowledge, investigations on structural thermal stability and oxidation resistance behaviours of these coatings via SR-XRD technique are yet to be established. This study addresses the temperature dependent surface morphology, mechanical properties, surface chemical bonding states, high temperature solar selective behaviours, and high temperature structural stability of magnetron sputtered TiAlSiN coatings via mechanical, SEM, XPS, UV-Vis and FTIR, and SR-XRD techniques.

2. Experimental techniques

2.1 Film deposition process

TiAlSiN films were deposited onto AISI M2 tool steel substrates via a closed field unbalanced magnetron sputtering system (UDP650, Teer Coating Limited, Droitwich, Worcestershire, UK). The magnetron sputtered system is equipped with a four-target

configuration. Before coating, the substrates were ultrasonically cleaned in an acetone and methanol solution and then dried using high purity nitrogen gas. A pressure of 0.24 Pa was maintained in the chamber throughout the deposition process. Prior to synthesizing the samples, all of the targets were cleaned properly and the steel substrates were safeguarded by shutters through the magnetrons. In order to achieve a homogeneous film thickness, the substrate was rotated at a speed of 10 rpm throughout the synthesis process. The substrates were sputter cleaned with Ar plasma at a bias of -450 V for 30 minutes. The coatings were deposited in an Ar+N_2 mixed gas atmosphere. The partial pressure of Ar and N_2 were 0.133 Pa and 0.106 Pa throughout the deposition processes. The bias currents for Ti, Al and Si target were 5 A, 7 A, and 5 A, respectively. The final products were then annealed at 500, 600, 700 and 800 °C. Details of the deposition conditions of TiAlSiN coatings are displayed in Table 1.

2.1 Characterisations

Scanning electron microscopy (SEM) was conducted to determine the surface morphology of the thin film coatings with a high resolution microscope (SEM, PHILIPS XL 20, Eindhoven, The Netherlands). A secondary electron (SEI) detector was used to characterize the overall surface morphology of thin film structures. The SEM machine was operated at 25 kV. The samples were glued with double sided carbon tape affixed to the sample holders.

A depth-sensing indentation system (Ultra-Micro Indentation System, UMIS-2000, CSIRO, Australia) equipped with a Berkovich indenter was used to measure the Young's modulus and hardness of the coatings. The indenter tip was calibrated by conducting single-cycling indentation tests on fused silica (a standard material having a known modulus of 72 GPa) at different loads. Load–unload tests were run in a closed-loop under load control to determine the mechanical properties of the samples. A maximum load of 20 mN was applied in 10 increments. The loading rate set to 2.5 mN/s represents the static response of the materials. Following each increment there were 10 decrements, from which the Young's modulus and hardness were calculated. Five indentation tests were performed on each specimen. The load vs displacement response obtained by nanoindentation is a very powerful technique for analysing mechanical properties. The elastic behaviour of, and deformation mechanisms within, the coating systems can be realized by analysing the nanoindentation data. In order to investigate the thermal stability of the sputtered films, mechanical hardness

of the coatings was tested with the samples before annealing and after being annealed between 500 °C and 800 °C in steps of 100 °C in air atmosphere.

The XPS data will reveal information on chemical structure, elemental compositions and bonding states in the outermost 5 nm surface of the films. The XPS measurements of the TiAlSiN coatings were taken using an XPS (Kratos Axis Ultra XPS spectrometer, Manchester, UK) machine operating with an Al-K_α monochromatic radiation ($h\nu$ = 1486.6 eV) source with a power of ~10 mA and ~15 kV. The XPS machine was also equipped with a cold stage, and an Ar ion gun for etching the coatings. The samples were mounted on a steel sample holder and put in the analysis chamber where the pressure was reduced to 2.9×10^{-9} Torr. The XPS survey spectra were collected before etching, and after 6 minutes etching. Ar ion sputtering was used for etching the films. Etching was done to remove any surface oxide layers and to reduce the Ti^{4+} ions in order to lower oxidation states. The high resolution XPS data was recorded after a 6 minute Ar^+ sputtering. The typical high resolution XPS core level spectra of TiAlSiN samples before and after being annealed show Ti2*p*, Al2*p*, Si2*p*, N1*s* and O1*s* energy regions. Information on the existence of various chemical bonding states was acquired by subtracting the background with the Shirley's method and deconvoluting the spectra with curve-fitting methods using CASA XPS software (version 2.3.1.5) [32].

The optical properties of the thin film coatings were analysed by measuring the optical reflectance as a function of wavelength from ultraviolet through the visible to infrared range of the solar spectrum via UV-Vis and FTIR spectrometers. A double-beam UV–Vis spectrophotometer (Model: UV-670 UV-Vis spectrophotometer, JASCO, USA) equipped with a unique, single monochromator design covering a wavelength range from 250 to 2500 nm was used to measure the solar absorptance of the coatings. The monochromator itself was designed with 1200 grooves/mm grating and a photo multiplier tube (PMT) detector. A PERKIN Elmer Spectrum 100 FTIR Spectrometer (USA) was used for measuring the reflectance, $R(\lambda)$, of the coatings in the wavelength range of 2.5 to 15 µm. Using the $R(\lambda)$ data the solar absorptance (α) and the solar emittance (ε) of a material can be conveniently estimated [20]. For a range of solar wavelengths, the total solar absorptance, α is defined as a weighted fraction between absorbed radiation and incoming solar radiation (I_{sol}), while thermal emittance, ε is defined as a weighted fraction between emitted radiation and the Planck black-body distribution (I_p). The figure of merit of a selective surface is expressed in term of a parameter known as the selectivity, *s*. The solar selectivity of a material is defined

by the ratio of the solar absorptance, α to the thermal emittance, ε, with expression (s) given in Ref. [20].

The SR-XRD measurements of the TiAlSiN coatings were carried out with the powder diffraction (PD) beamline 10-BM-1 at the Australian Synchrotron, in Melbourne. The PD beamline operated at 2.5 GeV and used a bending magnet source. A continuous spectrum of photons were generated in the range 5–30 keV with a maximum flux of about 10^{13} photons/sec and a beam size of 1 mm (W) × 8 mm (L) x 1 mm (H). The general beam size of the sample for the focused and unfocussed beam arrangements was 0.5 mm × 0.5 mm and 5 mm × 2 mm respectively. An X-ray wavelength of 0.8265 Å, estimated with a LaB6 standard NIST 660a, was used for the measurements. The high temperature system was an Anton Parr HTK20 furnace. The furnace was calibrated and monitored by a thermocouple and the heating and cooling cycles were remotely controlled via a computer interface. The high resolution XRD data was acquired at room temperature, 500 ℃, 600 ℃, 700 ℃, and 800 ℃. A MYTHEN II microstrip detector system was used to record the high resolution XRD data in the range of 2θ = 15° to 35° in steps of 0.02°. At each detector setting SR-XRD data was acquired for a period of 5 minutes. Data collection was started after a 3 min thermal equilibration period at which the control sensor had reached the set temperature. The acquired data was processed with PDViPeR software for further analysis.

3. Results and discussion

3.1 Surface morphology of TiAlSiN films

SEM images of sputtered TiAlSiN coatings before annealing and after being annealed at 500-800 ℃ in steps of 100 ℃ are presented in Fig. 1. SEM examination of the microstructure showed nanocomposite-like structure deformed by formation of an amorphous phase and facilitated by fine grains. As the annealing temperature progresses from 500 to 600 ℃, there originated some random pores around the surface of the coatings together with non-uniform grains. At the same time, the surface morphology and shape of the grains of the films were altered together with the rise in irregular mound like structures around the film's surfaces. Further inspection confirms that the higher surface roughness is attained by the coatings as the annealing temperature is increased. This surface roughness hinders the diffusion of titanium and nitrogen atoms and slows down their diffusions, helps to grain growth and develop amorphous like structures around the grain boundaries. However, the new phase is extremely small in size and cannot be detected by either XRD or SEM. Because of this lower mobility, the crystallization process is disrupted and disordering is enhanced for

195 further amorphization by Si_3N_4 phases around the boundaries. This amorphous grain
196 boundaries influence the optical properties of these coatings [33]. The annealed films
197 exhibited nanolayers which are observed as darker and lighter contrasts in the SEM
198 micrographs together with the fine-grained structure of the coatings. This is due to the
199 systematic increase on the oxide thickness growing on top of the coating with the rise in
200 annealing temperatures. The oxides layers which are observed are composed of Al_2O_3 and
201 SiO_2 at the outermost layer of the coating followed by TiO_2 layers (as seen in XPS studies).
202 These nano-sized protective layer formed on the nitride film hinders the diffusion of oxygen
203 into the coating due to their small size and polycrystalline nature. These nanolayers did not
204 vanish or alter their structure as a consequence of the heat treatment; rather, they seem to be
205 very stable [34]. The dense and closely packed structures show more stability as selective
206 surfaces at high temperatures. These kind of sputtered coatings are more reliable than similar
207 coatings with large columns and open pores [35]. These microstructural features have
208 substantial impacts on the residual stress and deformation mechanisms in the coatings and
209 could assist with the interpretation of mechanical hardness of these coatings.
210

211 **3.2 Mechanical properties of TiAlSiN coatings before annealing and after being**
212 **annealed**

213 The hardness, *H* and Young's modulus, *E* values of the sputtered TiAlSiN coatings
214 before and after annealing are presented in in Fig. 2. Table 2 represents the hardness, elastic
215 modulus, Yield strength and corresponding plastic deformation resistance of the TiAlSiN
216 coatings as acquired from the nanoindentation measurements. Before annealing, the TiAlSiN
217 coating showed a hardness of 28.1 ± 0.6 GPa and an elastic modulus of 369 ± 9 GPa. Similar
218 values for hardness and modulus have been reported in other studies [36-38].
219

220 The high hardness and high elastic modulus of TiAlSiN coatings before annealing
221 arises due to the biaxial compressive stress developed by high energetic ions bombardment
222 during the coating deposition. Effects of biaxial compressive stress on the hardness of
223 superhard multilayer coatings were examined by Veprek et al [39-41]. An increase in the
224 development of the intergranular amorphous phase in the nanocomposite matrix leads to a
225 definite enhancement of the hardness of the coatings. This is also true of the elastic modulus
226 values. At nano-scale level, the obstruction of dislocation movements and the nonappearance
227 of dislocations also contribute to enhance the hardness of the coatings [42]. The dissolution
228 of Al and Si atoms in the TiN crystallites produce solid solutions that are also responsible for

the greater hardness of these coatings [43, 44]. In addition, the grain boundary strengthening at interphase boundaries also predominate to a higher hardness in the films [37, 45]. According to Veprek [39-41], a superhard microstructure with high elasticity and thermal stability can be formed by fine nanocrystallites (<10 nm) enclosed by a thin amorphous phase (<1 nm) along with a strong boundary between the amorphous and crystalline phases. This interface successfully hinders the grain boundary sliding's, the formation of dislocations and their movements, and the spread of cracks. Generally a hard material has high wear resistance. The material's hardness and elastic modulus are also related to the wear behavior [46]. It is known that the wear of a material is coupled with the elastic limit of materials that define the ability of a material to deform under an applied stress and regain its initial state without being deformed permanently [46]. Experimental value of the elastic limit is expressed by the H/E ratio. The H^3/E^2 ratio, which is known as the plastic deformation factor, indicates the coating's resistance to plastic flow [47]. Each of the parameters play an essential role in the coating wear behaviors. The linear decrease of H, H/E and H^3/E^2 are well correlated with the reduction of wear resistance of TiAlSiN coatings during high temperature annealing. A high value of the H^3/E^2 ratio of a coating means that it offers high resistance to plastic deformation. This high value of the H^3/E^2 ratio is also associated with hindering dislocation formation or movement due to nano-grains and the solid impeding of the crack dissemination in the amorphous Si_3N_4 phase [48]. From an engineering application viewpoint, coating hardness must be accompanied by appropriate toughness and the ability of a material to absorb energy under an applied stress until fracture [49]. Musil and Jirout [50] reported their findings that resistance against crack formation of thin film coatings increases with increasing H^3/E^2 ratio. From Table 2, it can be seen that both the hardness and elastic modulus strongly depend on the annealing temperatures. The hardness decrement of the TiAlSiN coatings at elevated annealing temperatures may result from diverse mechanisms. Since the coatings were heated in air, the composition at the surface is expected to change due to oxidation, and therefore, it is reasonable to have lower hardness as the annealing temperature is enhanced. At high temperature annealing, the reduction in hardness and elastic modulus values of TiAlSiN coatings may be also ascribed to the softening of steel substrates, changes in composition of the films due to the diffusion, formation of new phases and stress relaxations. High temperature annealing causes grain refinement, and when combined with the formation of point defects, interstitials, biaxial compressive stress, and other effects of the ion bombardment may result in a reduction of hardness and elastic modulus as the temperature is increased. According to Petrov et al. and Barna et al., oxygen and other

impurities can lead to the grain refinement and alter the grain morphology of the coatings which also results to grain boundary embrittlement [51, 52]. Thus, the precise mechanism of the decrease of hardness and elastic modulus values with the rise in annealing temperature is not clear.

3.3 Atomic compositions and surface chemical bonding states of TiAlSiN thin film coatings

The elemental compositions of the TiAlSiN coatings were determined via XPS survey scans shown in Fig. 3. The detailed atomic compositions of these coatings, before annealing and after annealing at 500, 600, 700 and 800 °C, extracted from XPS survey spectra are outlined in Table 3. The existence of Ti, Al, Si, N, and O were identified following repeated XPS measurements of the deposited films.

The results show that annealing significantly affects the elemental compositions of these coatings. The atomic percentages of the constituent elements (Ti, Al, Si, N) are decreasing as the annealing temperature is increased; however the oxygen contents of the coatings were increased linearly. At 800 °C the Si2*p* and N1*s* signal were completely lost. This indicates that surface oxidation occurred at high temperatures. Since the oxygen content is higher at high annealing temperature, the oxidation layer may be thicker and more predominant at the surface. The specimens were etched with Ar+ for 6 minutes in order to remove the contamination. The XPS data acquired from these tests was calibrated with respect to the C1*s* peak at a standard binding energy of 284.6 eV, in order to make a correction for the charge shift.

The surface chemical bonding states of films were characterized by curve fitting of high resolution XPS data which were recorded after 6 minutes of etching. High resolution XPS spectra of the characteristic Ti*2p*, Al*2p*, Si*2p*, N*1s*, and O*1s* peaks before and after annealing are shown in Figs. 4-8. The existence of oxygen peaks exposes the existence of residual oxygen in the vacuum chamber and subsequent oxidation followed by the annealing in air atmosphere. High resolution Ti*2p*, Al*2p*, Si*2p*, N*1s*, and O*1s* peaks were deconvoluted to approximate the relative contributions of metal nitride and metal oxide related components to the coatings. The photoelectron lines, bonding states and their corresponding binding energy positions, FWHM values, and percentages of the components present in the coatings before annealing and being annealed at various temperatures as assessed from XPS curve fittings are displayed in Table 4.

The deconvolution curves of the high resolution XPS spectra of Ti$2p_{3/2}$ photoelectron lines are presented in Fig. 4. In TiAlSiN coatings the deconvolution of Ti$2p_{3/2}$ spectrum can

be allocated to three bonding states in the energy range of 455.1-458.6 eV. The peaks seen at 455.1-455.2 eV (labelled 'i') correspond to Ti-N/TiAlN/TiSiN/TiAlSiN phase, the peak at 456.6 eV (labelled 'ii') is related to Ti_2O_3 bonds and another peak at 458.6 eV (labelled 'iii') may be attributed to suboxides based on Ti_2AlO_5 or TiO_2 compounds. This reveals that the surface oxidation is initiated in these coatings while the peak broadening at higher annealing temperature confirms the appearance of reduced Ti ions. As a result of these peak broadenings, formation of bonding states of Ti-Al(N) and Ti-AiSi(N) phases are also predicted. It is also expected that some Ti may occur as Ti^{3+} ions in the form of TiN.

The deconvolution of Al2*p* spectra (Fig. 5) demonstrates two sub-peaks in the energy range of 72.6-75.3 eV. The first components are observed within 74.0-74.6 eV (labelled 'i'), the second components were seen around 75.0-75.3 eV (labelled 'ii'). The first features detected in the binding energy range of 74.0-74.6 eV are assumed to be the contribution of AlN structure. The second contribution is due to the occurrence of Al_2O_3 phase [53]. From the XPS fitting curves of these spectra it is revealed that the major portion of the Al2*p* spectrum is occupied by AlN phase.

Fig. 6 shows the Si2*p* core level photoelectron lines of TiAlSiN thin film coatings. Deconvoluting the Si2*p* core-level spectra by the curve-fitting method, we assessed the relative contributions of various phases to the total photoelectron signals in the sputtered coatings before and after annealing. The Si2*p* core level XPS spectra are fixed with two fragments within the energy range of 101.5-102.7 eV. The first segments at 101.5-101.8 eV (labelled 'i') are due to Si_3N_4 structure while the second peaks detected around 102.5-102.7 eV (labelled 'ii') are from O_2/Si or SiO_2 phase. Throughout the observations, all the Si atoms were bonded smoothly and demonstrated stoichiometric compositions with various stable structures.

The N1*s* photoelectron lines of TiAlSiN films before and after annealing are shown in Fig. 7. The curve fitting of N1*s* core level XPS spectra exhibited three constituents in the energy range of 396.5-398.5 eV. The first components in the binding energy range of 396.5-396.7 eV (labelled 'i') are related to nitrogen in TiN via TiN/TiAlN bonds, the second fragment at 397.3-397.6 eV (labelled 'ii') arise from the AlN phase and the relatively low intense third peak centred at 398.3-398.5 eV (labelled 'iii') are due to the presence of TiO_xN_y and/or the $Ti(Al/Si)O_xN_y$ phase.

Fig. 8 shows the O1*s* core level XPS spectra before and after annealing. Fitting the O1*s* XPS spectra consisted of three components in the binding energy range of 530.4-532.7

eV. The first features seen at 530.4-530.7 eV (labelled 'i') are applicable to the O_2/Ti or the TiO_2 phase, the second component detected within the binding energy positions of 531.2-531.7 eV (labelled 'ii') are apportioned as O_2/Ti or O_2/Al or O_2/Si phases while the third fragment observed around 532.3-532.7 eV (labelled 'iii') originated from the TiON or SiO_2 phases.

The deconvoluted XPS spectra of Ti2$p_{3/2,}$ Al2*p*, Si2*p*, N1*s* and O1*s* photoelectron lines reflect the fact that no significant changes in the binding energy features of these photoelectron lines were detected with respect to the increase in annealing temperatures. Accordingly, good structural and chemical stability of these films were achieved at high temperature annealing which is responsible for superior optical behaviours.

3.4 Solar selectivity sputtered TiAlSiN thin films

The UV-Vis reflectance spectra of the TiAlSiN coatings before annealing and after being annealed at 500-800 ℃ in steps of 100 ℃ are demonstrated in Fig. 9. In the visible spectrum range, the solar absorptance, α of these coatings was estimated by the Duffie and Beckman method [20]. In the Duffie-Beckman method, the estimated solar absorptance is an average value calculated from 20 values corresponding to the solar spectrum range between 190 nm and 2500 nm. The UV-Vis spectra reveals that all of the films demonstrate moderate reflectance up to 60 % to UV light, high absorptance above 90 % in the visible spectrum and exceptionally high reflectance (>98 %) in the infrared~far-infrared region of the solar spectrum. In the 400-650 nm range, all of the coatings display sharp absorption edges. It was also seen that the reflectivity of the coatings is decreased systematically as the annealing reaches up to 700 ℃ and then increased at 800 ℃. Above the visible range, the reflectance was enhanced gradually over the infrared range up to 2500 nm. The highest absorption of solar radiation was documented in the visible spectrum and the lowest absorptance in the infrared region. Similar absorptance features on TiN-based sputtered coatings were reported by Brogren et al. [54]. The high absorptance of the coating makes it an ideal candidate for selective solar surfaces to be used in the solar thermal collectors. The increase in solar absorption at high temperature annealing may be also associated with the gradual increase in the refractive index of the films from the surface to the substrate. In the case of single layered films on steel substrates, we achieved the highest solar absorptance of just over 84% and we believe that this can be substantially enhanced by designing multilayered transition metal nitride coatings. The addition of an antireflection layer on the top of film surface can also increase the light absorption ability of these coatings.

The FTIR reflectance spectra of the TiAlSiN thin film coatings before and after annealing are shown in Fig. 10. The solar absorptance, emittance and their before and after annealing are shown in Table 5. The results show the thermal emittance of the coatings decrease with the rise in annealing temperatures up to 600 °C while a significant declination of emittance was recorded for the coatings annealed at 700 and 800 °C. The absorptance values of the coatings were found to be increasing up to 700 °C while the emittance values were decreasing until 600 °C. Accordingly, the coatings have very high thermal stability in air up to 600 °C together with a high solar selectivity value of 23.9. The high thermal stability of these coatings in air up to 600 °C is due to several factors. Firstly, TiAlN works as a diffusion hurdle for steel. The formation of various metal oxides and nitrides phases (e.g., Ti_2O_3, Al_2TiO_5, TiN, AlN, and Si_3N_4 as seen in XPS results) at high temperatures conveniently stops the diffusion pathways for steel and thus acts as ideal diffusion barrier [55]. Thermal emittance is dependent on the surface oxide layers of these coatings. Higher infrared reflectivity of aluminium contributes to strengthen the oxidation behaviour of Al as observed around the Al2*p* spectrum. TiON with a stable phase and a very high melting point also acts as a diffusion barrier. In view of the above features, the TiAlSiN sputtered coatings display good thermal stability and preserve their optical properties even at higher annealing temperatures. At the same time, other factors such as the microstructure and the surface roughness of the films also influence the scattering, and the reflection of light. As annealing progresses from 600 °C to 800 °C, the emittance values decline because of the formation of the thick surface oxide layers that result in high infrared reflectivity [56].

The α/ε ratio is known as the solar selectivity, s. It characterizes the spectral features of a selective solar surface and is used in many solar thermal collector devices. The solar selectivity values of our coatings before and after annealing at various temperatures are set out in Table 6. The solar selectivity of TiAlSiN coatings is enriched significantly with the increase in annealing temperature up to 600 °C. The solar selectivity values of these coatings depend on a number of factors such as the thicknesses of the films, their structure, chemical compositions, relative content of individual phases, materials used, processing techniques, processing conditions, and the reflective nature of the substrate used. Thus, high temperature annealing effectively helps the formation of stable multiple crystalline and non-crystalline structures as seen in SR-XRD and XPS studies, stable chemical bonding states (as observed in XPS results) and thereby enhances the solar selectivity of these films. Moreover, the variation in structural morphology and elemental compositions might also help the surface

roughness of the films to enhance their selectivity values. Consequently, the overall solar selectivity of these coatings is boosted up to annealing of 600 °C.

3.5 In-situ SR-XRD studies of TiAlSiN coatings up to 800 °C

The TiAlSiN sputtered coatings were analysed by SR-XDR from room temperature then 500-800 °C in steps of 100 °C. The scan diffraction angle was between 2θ = 15° and 35°. The SR-XRD analysis results are presented in Fig. 11. As seen in Fig. 10, there is no apparent change in the patterns from room temperature up to 600 °C. However from 700 °C between 2θ = 22 and 35°, new peaks appear and some peaks disappear. Furthermore, the intensities of the peaks were also modified and peak widths were decreased. Gradual sharp and insignificant shifting of the peak positions at higher annealing temperatures indicate the formation of stable microstructures resulting from isostructural decomposition to form Ti-rich, Al-rich and Si-rich phases via spinodal decompositions [57, 58]. This also demonstrates the fact that TiAlSiN coatings retain decent structural and chemical stability within the operating temperature up to 800 °C. Analysis of the SR-XRD data established that the sputtered TiAlSiN coatings were made up of crystalline TiN, AlN, Si_3N_4, Al_2O_3, and Fe (substrate) phases. The 2θ positions, crystal phases, Miller indices and space groups of sputtered TiAlSiN coatings from SR-XRD are set out in Table 7. The 2θ positions of the existing phases are very close to each other at all temperatures. The formations of h-AlN and h-Si_3N_4 phases are evidence of the spinodal decomposition of these coatings. This spinodal decomposition [59] is responsible for the grain refinement and modifications of microstresses within AlN and Si_3N_4 domains. The modification of peak intensities suggests that a higher degree of crystallinity is achieved when the films are annealed at high temperatures. At 800 °C two of the Fe based peaks (due to the substrate) disappear indicating that a phase transition has occurred in the substrate. This is not unexpected as the Fe phase diagrams show phase changes above 600 °C.

Generally the formation of an Al_2O_3 layer on the surface of coatings prevents the penetration of oxygen into the specimen as temperature is raised, thereby increasing the crystal stability at high temperature working environments [60]. These features are also associated with the difference in atomic radii of the constituent elements together with the bond coordination, and the preferred crystallographic network of the films. The compact Al_2O_3 layer obstructs the inward diffusion of oxygen and the outward diffusion of Ti, Al and Si and thereby improves the oxidation resistance of TiAlSiN coatings. According to Chen et

al. [61], in TiN and TiAlN coatings surface oxidations were detected at 700 and 800 °C and the substrate started to oxidize at 800 and 900 °C respectively. However, TiAlSiN coatings can prevent oxidization up to 900 °C. This is probably due to the formation of thin dense oxide layers around the surfaces of the films that protects them from being further oxidized. The influence of temperature is not only related to the formation of stable phases and oxygen contamination but also to the morphology and growth mode of the films that it also affects the solar selectivity of the films.

Data from XRD are from the bulk substrate/film as the x-rays penetrate through thickness of many micrometers (μm) while the XPS data is from penetration of only a few nanometres (nm). At 800 °C, combining the XPS and XRD results together, it is certain that the top layer of the sample consists of Ti and Al oxides and no nitrides while the rest of the film consists of Ti, Al and Si oxides and nitrides. Fig. 12 is a schematic diagram showing the general region of the oxide and nitride phases at this temperature. At temperatures below 800 °C the entire thin film consists of oxide and nitride phases as listed in Table 6.

4. Conclusions

State-of-the-art magnetron sputtered TiAlSiN thin films, on a M2 steel substrate, were investigated, before and after annealing over temperature range of 500 °C to 800 °C, for their structural, microstructural morphology, mechanical properties, surface chemical bonding states and solar selective behaviours. Images from SEM analysis show nanolayers forming dense and closely packed structures with amorphous grain boundaries. Increasing annealing temperature results in higher surface roughness of the thin films. These indicate the sputtered films have good stability and increased reliability than similar coatings with large columns and open pores. Mechanical studies show a decrease of hardness, Young's modulus, plastic deformation and constant yield strength, in the above temperature range, for the coatings. These displayed good wear resistance which is dependent on better oxidation and thermal stability initiated from amorphous boundaries to slow down the interface reaction and recrystallization in the annealing cycle. No significant changes in the binding energies of the Ti2*p*, Al2*p*, Si2*p*, N1*s* and O1*s* photoelectron lines were detected from the XPS studies of the films. The XPS results indicate mixed Ti, Al and Si nitrides and oxides as main film components but at 800 °C the top layer, of the thin film, is clearly composed of Ti and Al oxides. The solar selectivity increased a maximum of 24.6, at 600 °C, and then substantially

decreased at higher temperatures due to formation of oxide phases at the top layer of the thin film coatings. This is in accordance with the general rule that solar selective coatings are affected by the stoichiometric compositions, and the annealing temperature. XRD analysis showed various Ti, Al and Si nitride and oxide phases, for the above annealing temperature range, with isostructural development of cubic Ti-rich, Al-rich and Si-rich domains. From 700 °C there are strong indications that a phase change is occurring with the Fe component in the substrate. Transition metal nitride based materials exhibited a variety of interesting structural, mechanical and optical properties and are expected to play growing roles in energy related applications, such as solar energy harnessing as solar selective surface. The XPS results obtained from the coating surface can not reveal the composition inside the coatings because; high temperature annealing was in air atmosphere, whereas oxygen is more prominent at the surface. Depth profile studies along the film thickness direction, will afford better understanding of the oxidation mechanisms as well as the possible diffusion and distribution of different elements of the sputtered coatings. The studies may even clarify any phase changes occurring in the substrate.

Acknowledgements

This research was supported by School of Engineering & Information Technology at Murdoch University. The authors gratefully acknowledge funding by the Australian Synchrotron beamtime award AS141/PD/7582. M. Mahbubur Rahman gratefully acknowledges Murdoch University for providing with the financial support under the Murdoch International Postgraduate Research Scholarship (MIPRS) program to carry out his PhD studies.

References

[1] A. Flink, T. Larsson, J. Sjölén, L. Karlsson, L. Hultman, Surface and Coatings Technology, 200 (2005) 1535-1542.

[2] C.G. Granqvist, Solar Energy Materials and Solar Cells, 91 (2007) 1529-1598.

[3] N. Selvakumar, H.C. Barshilia, Solar Energy Materials and Solar Cells, 98 (2012) 1-23.

[4] H.C. Barshilia, N. Selvakumar, K.S. Rajam, A. Biswas, Solar Energy Materials and Solar Cells, 92 (2008) 1425-1433.

[5] H.C. Barshilia, N. Selvakumar, K.S. Rajam, A. Biswas, Solar Energy Materials and Solar Cells, 92 (2008) 495-504.

[6] M. Du, L. Hao, J. Mi, F. Lv, X. Liu, L. Jiang, S. Wang, Solar Energy Materials and Solar Cells, 95 (2011) 1193-1196.

[7] S.A. Kalogirou, Progress in Energy and Combustion Science, 30 (2004) 231-295.

[8] C.E. Kennedy, H. Price, Proceedings of ISEC 2005, 520 (2005).

[9] Y. Liu, C. Wang, Y. Xue, Solar Energy Materials and Solar Cells, 96 (2012) 131-136.

[10] C. Nunes, V. Teixeira, M.L. Prates, N.P. Barradas, A.D. Sequeira, Thin Solid Films, 442 (2003) 173-178.

[11] N. Selvakumar, N.T. Manikandanath, A. Biswas, H.C. Barshilia, Solar Energy Materials and Solar Cells, 102 (2012) 86-92.

[12] S. Yue, S. Yueyan, W. Fengchun, Solar Energy Materials and Solar Cells, 77 (2003) 393-403.

[13] H.C. Barshilia, Solar Energy Materials and Solar Cells, 130 (2014) 322-330.

[14] L. Hao, S. Wang, L. Jiang, X. Liu, H. Li, Z. Li, Chinese Science Bulletin, 54 (2009) 1451-1454.

[15] H.C. Barshilia, N. Selvakumar, K.S. Rajam, D.V. Sridhara Rao, K. Muraleedharan, Thin Solid Films, 516 (2008) 6071-6078.

[16] N. Selvakumar, H.C. Barshilia, K.S. Rajam, A. Biswas, Solar Energy Materials and Solar Cells, 94 (2010) 1412-1420.

[17] A. Amri, X. Duan, C.Y. Yin, Z.T. Jiang, M.M. Rahman, T. Pryor, Applied Surface Science, 275 (2013) 127-135.

[18] A. Amri, Z.T. Jiang, P.A. Bahri, C.Y. Yin, X. Zhao, Z. Xie, X. Duan, H. Widjaja, M.M. Rahman, T. Pryor, Journal of Physical Chemistry C, 117 (2013) 16457-16467.

[19] A. Amri, Z.T. Jiang, X. Zhao, Z. Xie, C.Y. Yin, N. Ali, N. Mondinos, M.M. Rahman, D. Habibi, Surface and Coatings Technology, 239 (2014) 212-221.

[20] A. Millar, M.M. Rahman, Z.-T. Jiang, Journal of Advanced Physics, 3 (2014) 179-193.

[21] A. Amri, Z.T. Jiang, N. Wyatt, C.Y. Yin, N. Mondinos, T. Pryor, M.M. Rahman, Ceramics International, 40 (2014) 16569-16575.

[22] A. Fardausy, M.A. Kabir, H. Kabir, M.M. Rahman, K. Begam, F. Ahmed, M.A. Hossain, M.A. Gafur, International Journal of Advanced Research in Engineering and Technology, 3 (2012) 267-274.

[23] M.M. Rahman, Z.-T. Jiang, Z. Xie, X. Duan, Z.-f. Zhou, P.C. Wo, C.-Y. Yin, N. Mondinos, Q. Gu, H. Widjaja, K. Jack, A. Yago, A. Amri, The Journal of Physical Chemistry C, 118 (2014) 18573-18579.

[24] M. Mahbubur Rahman, A. Duan, Z.-T. Jiang, Z. Xie, A. Wu, A. Amri, B. Cowie, C.-Y. Yin, Journal of Alloys and Compounds, 578 (2013) 362-368.

[25] M.M. Rahman, Z.-T. Jiang, X. Duan, Z. Xie, A. Tadich, Z.-f. Zhou, N. Mondinos, C.-Y. Yin, M. Altarawneh, B.Z. Dlugogorski, Journal of Alloys and Compounds, 661 (2016) 268-273.

[26] S. Veprek, H.D. Männling, M. Jilek, P. Holubar, Materials Science and Engineering A, 366 (2004) 202-205.

[27] S.K. Kim, P.V. Vinh, J.H. Kim, T. Ngoc, Surface and Coatings Technology, 200 (2005) 1391-1394.

[28] H.C. Barshilia, N. Selvakumar, K.S. Rajam, D.V. Sridhara Rao, K. Muraleedharan, A. Biswas, Applied Physics Letters, 89 (2006) 1919.

[29] X. Orignac, D. Barbier, X.M. Du, R.M. Almeida, Applied Physics Letters, 69 (1996) 895-897.

[30] R.M. Almeida, X. Orignac, D. Barbier, J Sol-Gel Sci Technol, 2 (1994) 465-467.

[31] Y. Sorek, R. Reisfeld, I. Finkelstein, S. Ruschin, Applied Physics Letters, 63 (1993) 3256-3258.

[32] D.A. Shirley, Physical Review B, 5 (1972) 4709-4714.

[33] J.H. Kang, K.J. Kim, Journal of Applied Physics, 86 (1999) 346-350.

[34] Z. Zhou, W.M. Rainforth, B. Rother, A.P. Ehiasarian, P.E. Hovsepian, W.D. Münz, Surface and Coatings Technology, 183 (2004) 275-282.

[35] M. Kotilainen, K. Mizohata, M. Honkanen, P. Vuoristo, Solar Energy Materials and Solar Cells, 120 (2014) 462-472.

[36] F.N. Khan, A. Daadbin, M. Persson, J. Haider, H. Hellbergh, Proceedings of the Institution of Mechanical Engineers, Part B: Journal of Engineering Manufacture, 226 (2012) 870-877.

[37] C.L. Chang, J.W. Lee, M.D. Tseng, Thin Solid Films, 517 (2009) 5231-5236.

[38] T. Mori, M. Noborisaka, T. Watanabe, T. Suzuki, Surface and Coatings Technology, 213 (2012) 216-220.

[39] S. Vepřek, Journal of Vacuum Science and Technology A: Vacuum, Surfaces and Films, 17 (1999) 2401-2420.

[40] S. Veprek, P. Nesladek, A. Niederhofer, F. Glatz, Nanostructured Materials, 10 (1998) 679-689.

[41] S. Vepřek, S. Reiprich, Thin Solid Films, 268 (1995) 64-71.

[42] S.Q. Wang, L. Chen, B. Yang, K.K. Chang, Y. Du, J. Li, T. Gang, International Journal of Refractory Metals and Hard Materials, 28 (2010) 593-596.

[43] D. Yu, C. Wang, X. Cheng, F. Zhang, Thin Solid Films, 517 (2009) 4950-4955.

[44] L. Chen, Y. Du, A.J. Wang, S.Q. Wang, S.Z. Zhou, International Journal of Refractory Metals and Hard Materials, 27 (2009) 718-721.

[45] J.S. Kim, G.J. Kim, M. Chang Kang, J.W. Kim, K.H. Kim, Surface and Coatings Technology, 193 (2005) 249-254.

[46] A. Leyland, A. Matthews, Wear, 246 (2000) 1-11.

[47] P.H. Mayrhofer, C. Mitterer, J. Musil, Surface and Coatings Technology, 174-175 (2003) 725-731.

[48] I.W. Park, S.R. Choi, J.H. Suh, C.G. Park, K.H. Kim, Thin Solid Films, 447-448 (2004) 443-448.

[49] S. Zhang, D. Sun, Y. Fu, H. Du, Surface and Coatings Technology, 198 (2005) 74-84.

[50] J. Musil, M. Jirout, Surface and Coatings Technology, 201 (2007) 5148-5152.

[51] I. Petrov, P.B. Barna, L. Hultman, J.E. Greene, Journal of Vacuum Science and Technology A: Vacuum, Surfaces and Films, 21 (2003) S117-S128.

[52] A. Barna, P.B. Barna, G. Radnoczi, F.M. Reicha, L. Toth, Physica Status Solidi (A) Applied Research, 55 (1979) 427-435.

[53] L. Rosenberger, R. Baird, E. McCullen, G. Auner, G. Shreve, Surface and Interface Analysis, 40 (2008) 1254-1261.

[54] M. Brogren, G.L. Harding, R. Karmhag, C.G. Ribbing, G.A. Niklasson, L. Stenmark, Thin Solid Films, 370 (2000) 268-277.

[55] Y.K. Lee, K.M. Latt, T. Osipowicz, C. Sher-Yi, Materials Science in Semiconductor Processing, 3 (2000) 191-194.

[56] D. Gong, X. Cheng, W. Ye, P. Zhang, G. Luo, Journal Wuhan University of Technology, Materials Science Edition, 28 (2013) 256-260.

[57] C. Feng, S. Zhu, M. Li, L. Xin, F. Wang, Oxidation of Metals, 71 (2009) 63-76.

[58] P.H. Mayrhofer, F.D. Fischer, H.J. Böhm, C. Mitterer, J.M. Schneider, Acta Materialia, 55 (2007) 1441-1446.

[59] J.T. Chen, J. Wang, F. Zhang, G.A. Zhang, X.Y. Fan, Z.G. Wu, P.X. Yan, Journal of Alloys and Compounds, 472 (2009) 91-96.

[60] M.S. Leu, S.C. Lo, J.B. Wu, A.K. Li, Surface and Coatings Technology, 201 (2006) 3982-3986.

[61] J.K. Chen, C.L. Chang, Y.N. Shieh, K.J. Tsai, B.H. Tsai, Procedia Engineering, 36 (2012) 335-340.

Table 1. Details of the deposition conditions of the magnetron sputtered TiAlSiN coatings.

Experimental Conditions	Name/Values
Empirical formula	$Ti_{0.5}Al_{0.2}Si_{0.05}N_{0.5}$
Formula weight	25.776 g/mol
Substrate	M42 Steel (HRC60)
Target materials	Ti + Al + Si targets
Reaction gas	Ar is working gas, N_2 is reactive gas
Substrate thickness	3 mm
Target to substrate distance	170 mm
Substrate temperature	500 ^{o}C
Substrate DC bias voltage	-55 V
Substrate holder rotation frequency	10 rpm
Ar flow rate	20 sccm
N_2 flow rate	Controlled by optical emission monitor, OEM = 35%
Ar partial pressure	0.133 Pa
N_2 partial pressure	0.106 Pa
(Ar + N_2) pressure	0.24 Pa
Operating pressure	0.24 Pa
Base/ultimate pressure	4×10^{-4} Pa
Ti target power	2 kW
Ti target current	6.0 A (DC)
Al target power	1.2 kW
Al target current	4.5 A (DC)
Si target power	460 kW
Si target current	1.5 A (DC)
Deposition rate	~2.2 nm/min
Deposition time	90 min
Thickness of the coating	~0.2 µm

Table 2. Mechanical characteristics of sputtered TiAlSiN films before annealing and after being annealed at different temperatures.

Annealing temperature (°C)	Hardness, *H* (GPa)	Young's modulus, *E* (GPa)	Yield strength, $\frac{H}{E}$	Plastic deformation factor, $\frac{H^3}{E^2}$ (GPa)
Before annealing	28.12 ± 0.6	369.1 ± 9	0.08	0.16
500	26.76 ± 0.5	360.6 ± 7	0.07	0.15
600	24.43 ± 0.3	341.2 ± 8	0.07	0.13
700	23.06 ± 0.3	328.2 ± 8	0.07	0.12
800	22.16 ± 0.4	312.8 ± 12	0.07	0.11

Table 3. Details of the elemental compositions of the as deposited-TiAlSiN and annealed unbalanced magnetron sputtered coatings acquired via XPS survey scans.

Annealing temperatures (°C)	Atomic percentages of the elements					
	Ti	Al	Si	N	C	O
As deposited	20.31	18.23	2.57	25.64	13.13	20.12
500	17.21	15.37	2.38	7.86	14.06	43.12
600	17.17	10.71	1.51	5.05	13.41	52.15
700	14.27	7.05	0.67	3.84	27.72	46.45
800	6.75	6.15	00	2.27	34.57	51.26

Table 4. Fitting results of the XPS data of TiAlSiN sputtered coatings for the core level binding energies.

Annealing temperature	Line	Bonding states	Binding energy (eV)	FWHM (eV)	Percentages of the component (%)
Before annealing	Ti2$p_{3/2}$	TiN/TiAlN/ TiSiN/TiAlSiN	455.1	1.1	35.0
		Ti_2O_3	456.6	1.5	22.9
		Al_2TiO_5 or TiO_2	458.6	1.7	15.3
	Al2*p*	AlN	74.2	1.0	60.6
		Al_2O_3	75.0	1.0	39.4
	Si2*p*	Si_3N_4	101.5	1.2	40.5
		O_2/Si or SiO_2	102.6	1.2	59.5
	N1*s*	TiN/TiAlN/ TiSiN/TiAlSiN	396.6	1.2	39.9
		AlN	397.3	1.1	48.7
		TiO_xN_y and/or $Ti(Al/Si)O_xN_y$	398.4	1.1	11.4
	O1*s*	O_2/TiN or TiO_2	530.5	1.7	51.4
		O_2/Ti or O_2/Al or O_2/Si	531.7	1.9	33.4
		TiON or SiO_2	532.7	1.7	15.2
500 °C	Ti2$p_{3/2}$	TiN/TiAlN/ TiSiN/TiAlSiN	455.1	1.2	27.6
		Ti_2O_3	456.7	1.2	39.2
		Al_2TiO_5 or TiO_2	458.5	1.2	33.2
	Al2*p*	AlN	74.0	1.1	67.4
		Al_2O_3	75.0	1.1	32.6
	Si2*p*	Si_3N_4	101.8	1.3	36.2
		O_2/Si or SiO_2	102.7	1.3	63.8
	N1*s*	TiN/TiAlN/ TiSiN/TiAlSiN	396.5	1.0	62.5
		AlN	397.6	0.9	16.2
		TiO_xN_y and/or $Ti(Al/Si)O_xN_y$	398.3	1.2	21.3
	O1*s*	O_2/TiN or TiO_2	530.7	1.1	44.5
		O_2/Ti or O_2/Al or O_2/Si	531.4	1.2	29.4
		TiON or SiO_2	532.4	1.7	26.1
600 °C	Ti2$p_{3/2}$	TiN/TiAlN/ TiSiN/TiAlSiN	455.1	1.3	27.2
		Ti_2O_3	456.4	1.3	32.0
		Al_2TiO_5 or TiO_2	458.4	1.3	40.8
	Al2*p*	AlN	74.1	1.1	62.5
		Al_2O_3	75.1	1.1	37.5
	Si2*p*	Si_3N_4	101.7	1.3	38.2
		O_2/Si or SiO_2	102.6	1.0	61.8
	N1*s*	TiN/TiAlN/ TiSiN/TiAlSiN	396.7	0.9	14.0
		Al_2TiO_5	397.3	1.2	78.9
		TiO_xN_y and/or	398.3	0.5	7.1

		$Ti(Al/Si)O_xN_y$			
	O1*s*	O_2/TiN or TiO_2	530.7	1.2	34.2
		O_2/Ti or O_2/Al or O_2/Si	531.3	1.3	39.3
		TiON or SiO_2	532.4	1.8	26.5
700 °C	Ti2$p_{3/2}$	TiN/TiAlN/ TiSiN/TiAlSiN	455.2	2.0	16.6
		Ti_2O_3	456.7	1.9	54.0
		Al_2TiO_5 or TiO_2	458.5	1.5	29.4
	Al2*p*	AlN	74.6	1.0	52.9
		Al_2O_3	75.3	1.0	47.1
	Si2*p*	Si_3N_4	101.7	1.2	41.5
		O_2/Si or SiO_2	102.5	1.2	58.5
	N1*s*	TiN/TiAlN/ TiSiN/TiAlSiN	396.6	1.1	23.2
		Al_2TiO_5	397.3	1.1	67.8
		TiO_xN_y and/or $Ti(Al/Si)O_xN_y$	398.5	0.6	9.0
	O1*s*	O_2/TiN or TiO_2	530.5	1.2	42.3
		O_2/Ti or O_2/Al or O_2/Si	531.2	1.6	48.9
		TiON or SiO_2	532.5	1.7	8.8
800 °C	Ti2$p_{3/2}$	TiN/TiAlN/ TiSiN/TiAlSiN	455.1	1.3	21.8
		Ti_2O_3	456.5	1.3	43.1
		Al_2TiO_5 or TiO_2	458.6	1.3	35.1
	Al2*p*	AlN	74.0	1.0	42.1
		Al_2O_3	75.0	1.2	57.9
	O1*s*	O_2/TiN or TiO_2	530.4	1.7	20.3
		O_2/Ti or O_2/Al or O_2/Si	531.4	1.6	47.4
		TiON or SiO_2	532.3	1.9	32.3

Table 5. Solar absorptance and thermal emittance of sputtered TiAlSiN coatings before annealing and after being annealed at 500, 600, 700, and 800 °C.

Annealing temperature (°C)	Solar absorptance, α before annealing	Solar absorptance, α after annealing	$\Delta\alpha$	Thermal emittance, ε before annealing	Thermal emittance, ε after annealing	$\Delta\varepsilon$
500	0.810	0.822	+0.012	0.0358	0.0344	+0.0014
600		0.830	+0.020		0.0337	+0.0021
700		0.844	+0.034		0.0488	-0.0130
800		0.798	-0.012		0.0528	-0.0170

Table 6. Solar selectivity of sputtered TiAlSiN coatings before annealing and after being annealed at 500, 600, 700, and 800 °C.

Annealing temperature (°C)	Solar absorptance, α	Thermal emittance, ε	Solar selectivity, $s = \alpha/\varepsilon$
Before annealing	0.810	0.0358	22.63
500	0.822	0.0344	23.90
600	0.830	0.0337	24.63
700	0.844	0.0488	17.30
800	0.798	0.0528	15.11

Table 7: 2θ Positions, crystal phases, Miller indices and space groups of sputtered TiAlSiN coatings as observed from synchrotron radiation X-ray diffraction (SR-XRD) studies.

2θ position at room temperature	2θ position at 500°C	2θ position at 600°C	2θ position at 700°C	2θ position at 800°C	Crystal structure	Miller Index	Space group	JCPDS reference
19.33 (A)	19.35	19.32	19.32	19.30	$TiN_{0.6}$/Tetragonal	(112)	14_1/amd(141)	76-1834
20.18 (C)	20.20	20.19	20.18	20.21		(103)		
26.09 (G)	26.10	26.11	26.13	26.09		(211)		
33.14 (I)	33.12	33.10	33.10	33.10		(220)		
19.55 (B)	19.58	19.54	19.52	19.51	TiN/Cubic	(111)	Fm-3m(225)	87-0633
22.26 (D)	22.28	22.28	22.26	22.25		(200)		
32.18 (H)	32.22	32.18	32.15	32.16		(222)		
19.33 (A)	19.34	19.33	19.32	19.30	AlN/Hexagonal	(002)	$P6_3mc$(186)	88-2360
20.18 (C)	20.18	20.19	20.20	20.18		(101)		
19.33 (A)	19.32	19.33	19.34	19.33	Si_3N_4/Hexagonal	(120)	$P6_3$(173)	82-0705
21.08 (B)	21.09	21.08	21.10	21.10		(111)		
26.09 (G)	26.09	26.08	26.11	26.12		(310)		
19.33 (A)	19.34	19.35	19.32	19.30	Al_2O_3/Rhombohedral	(104)	R-3c(167)	88-0826
22.59 (E)	22.58	22.57	22.55	22.55		(113)		
23.26 (F)	23.25	23.25	23.23	23.20	Fe/Cubic	(110)	lm-3m(229)	85-1410
33.14 (I)	33.13	33.12	33.10	33.10		(211)		

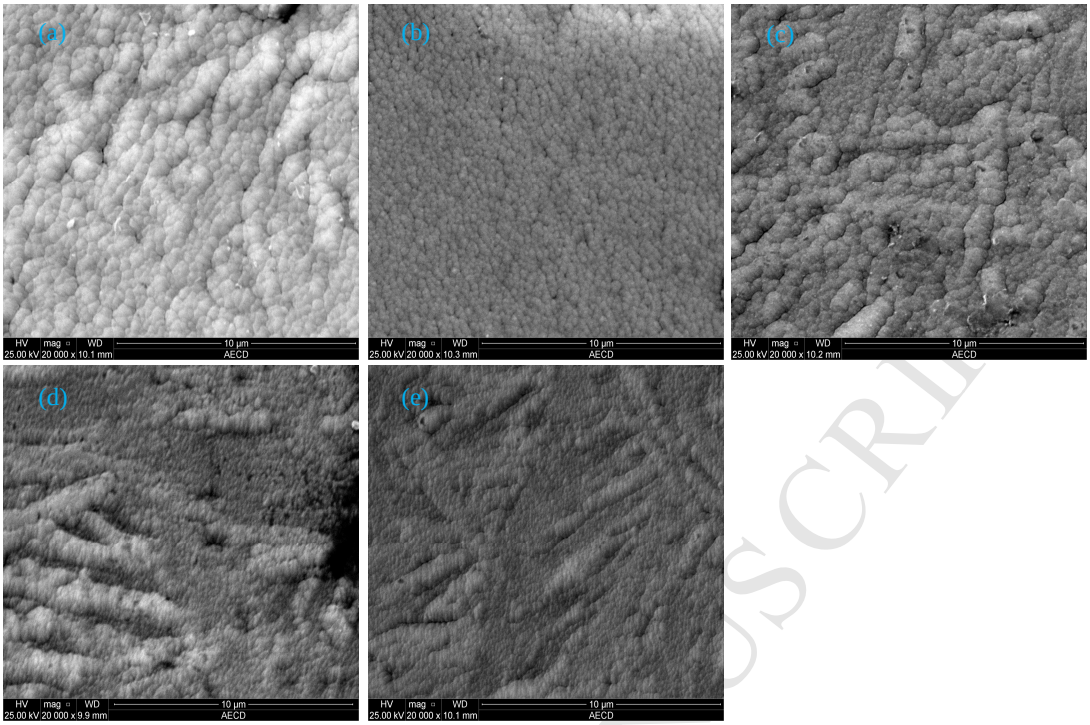

Figure 1. SEM micrographs of: (a) TiAlSiN coating before annealing and after being annealed at (b) 500 °C, (c) 600 °C, (d) 700 °C, AND (e) 800 °C, temperatures respectively.

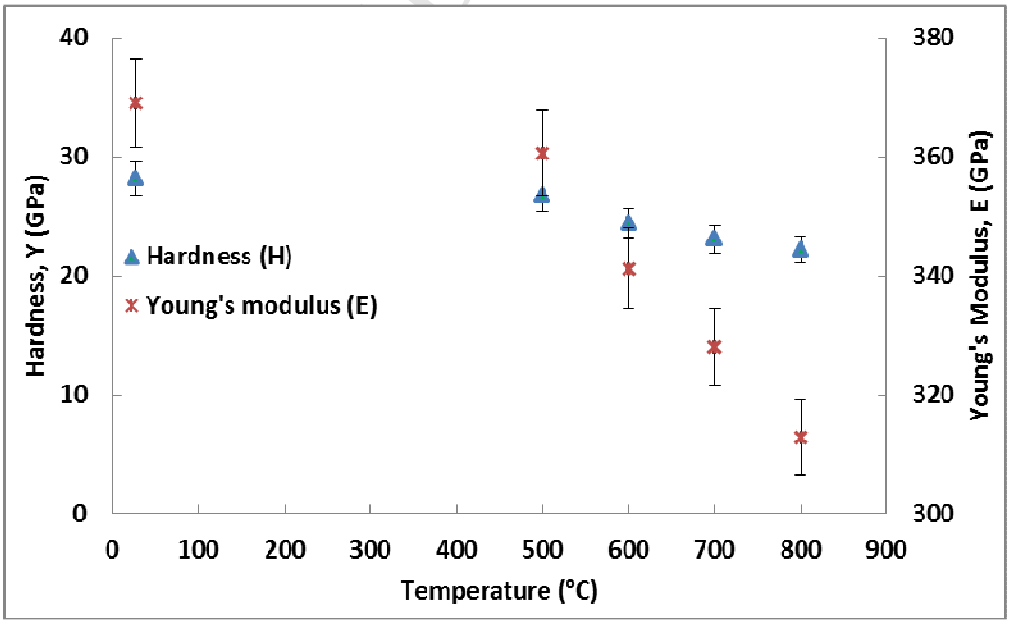

Figure 2. Mechanical parameters of TiAlSiN coating before annealing and after being annealed at 500-800 °C in steps of 100 °C.

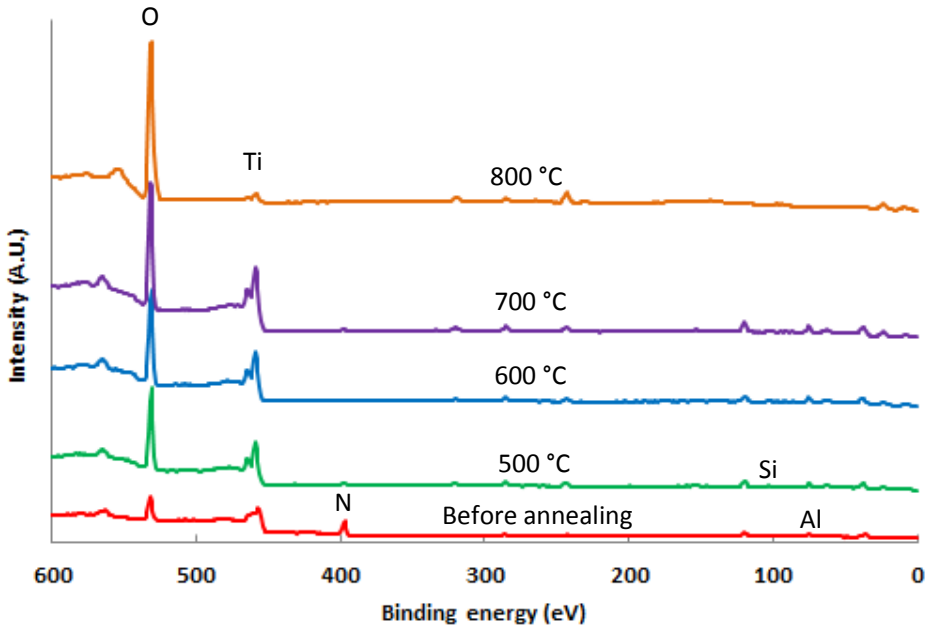

Figure 3. XPS survey scans of magnetron sputtered TiAlSiN coatings before annealing and after being annealed at 500-800 °C in steps of 100 °C.

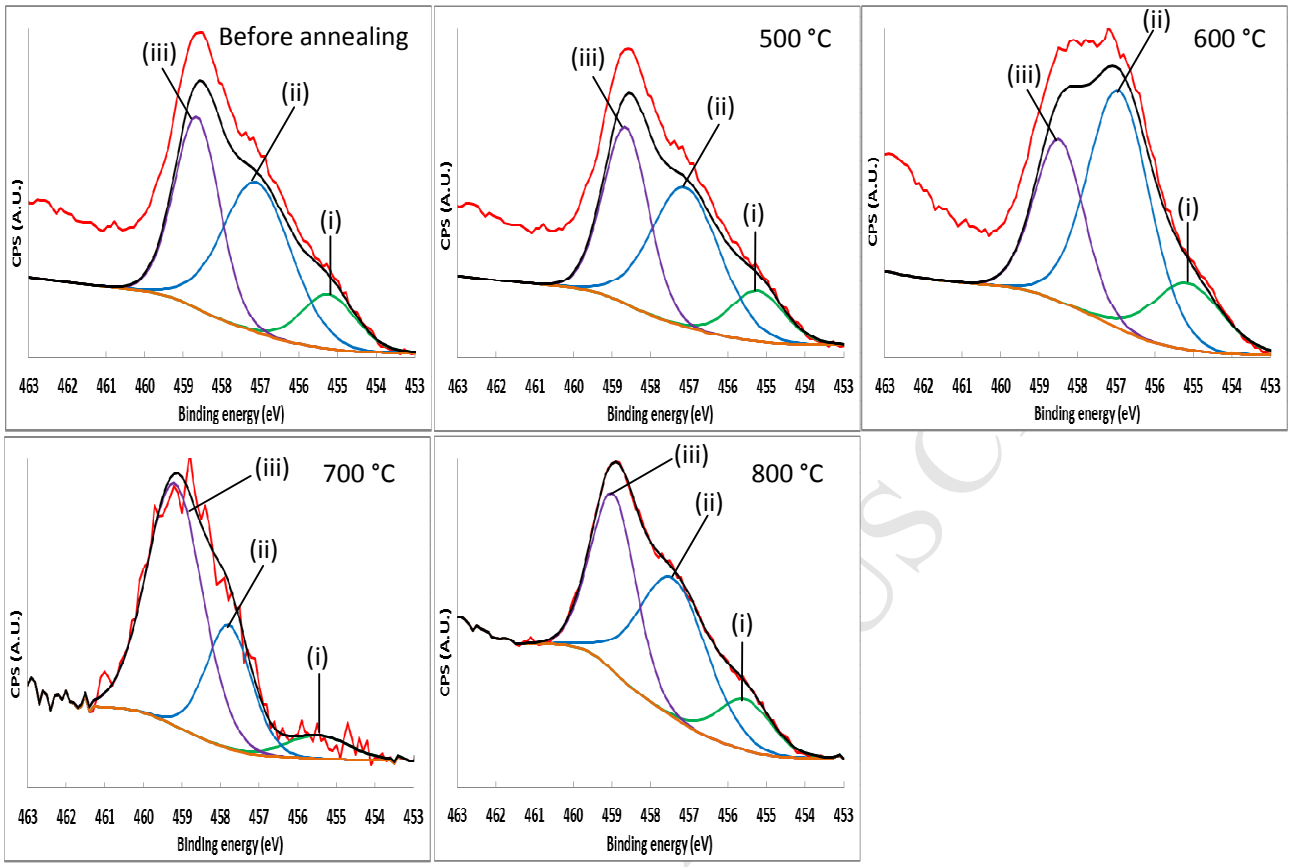

Figure 4. Typical fitting curves of Ti2$p_{3/2}$ XPS spectra of sputtered TiAlSiN coatings before annealing and after being annealed at various temperatures.

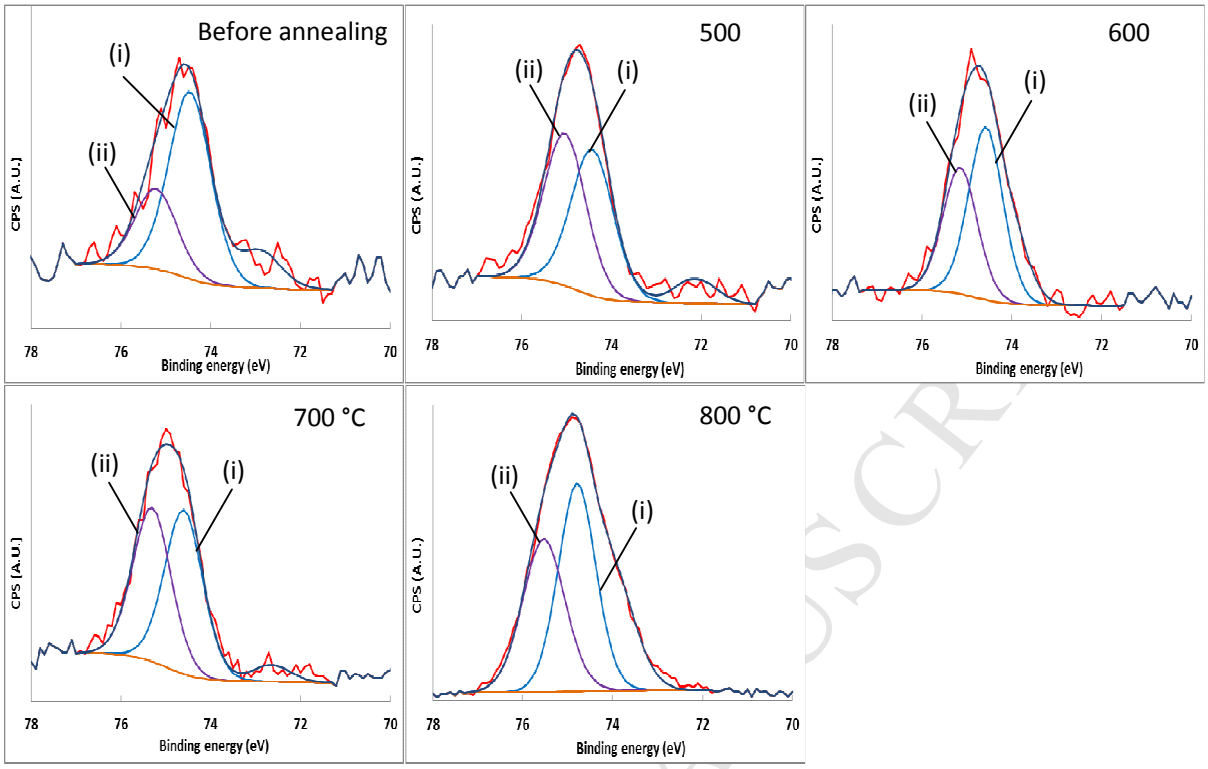

Figure 5. Typical fitting curves of Al2*p* XPS spectra of sputtered TiAlSiN coatings before annealing and after being annealed at various temperatures.

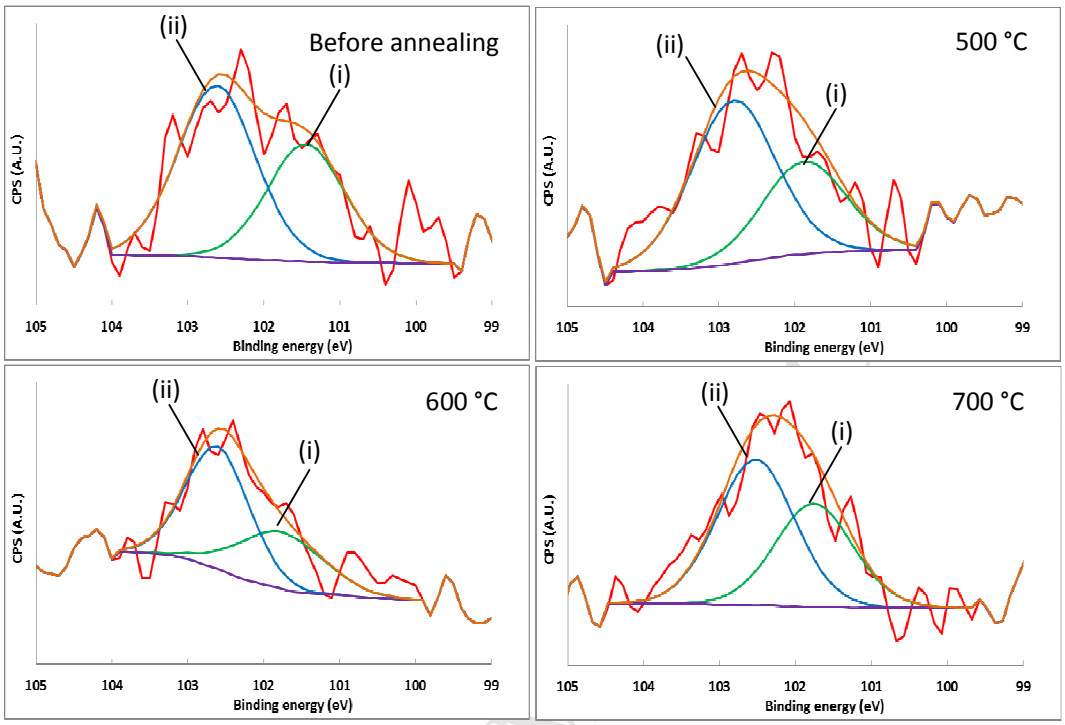

Figure 6. Typical fitting curves of Si2*p* XPS spectra of sputtered TiAlSiN coatings before annealing and after being annealed at various temperatures.

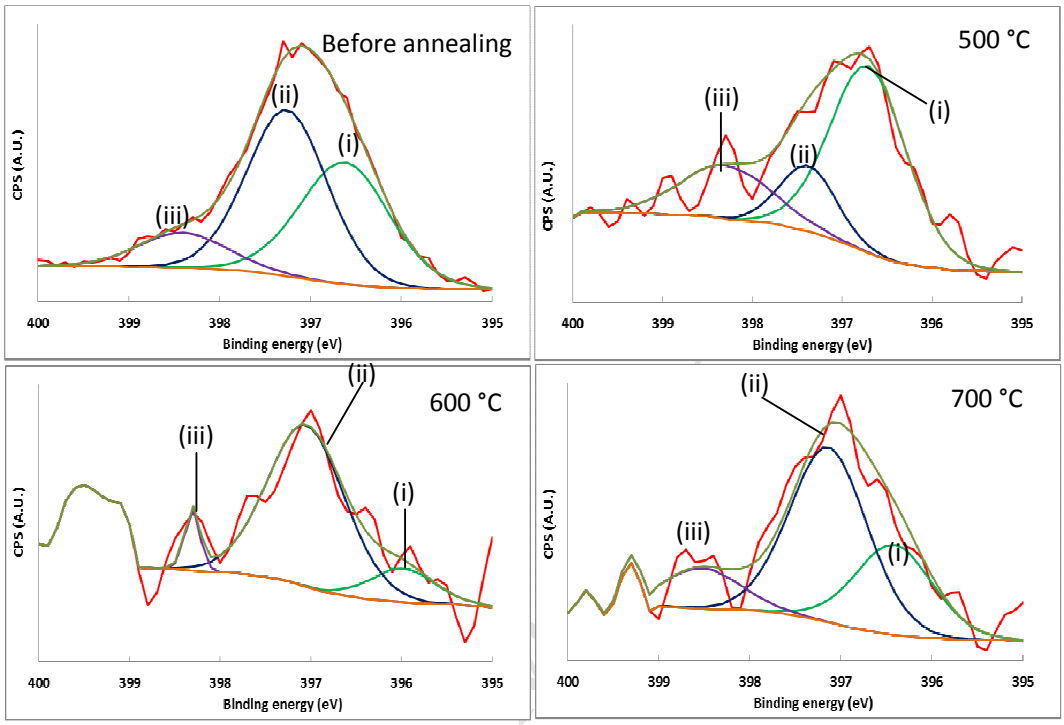

Figure 7. Typical fitting curves of N1*s* XPS spectra of sputtered TiAlSiN coatings before annealing and after being annealed at various temperatures.

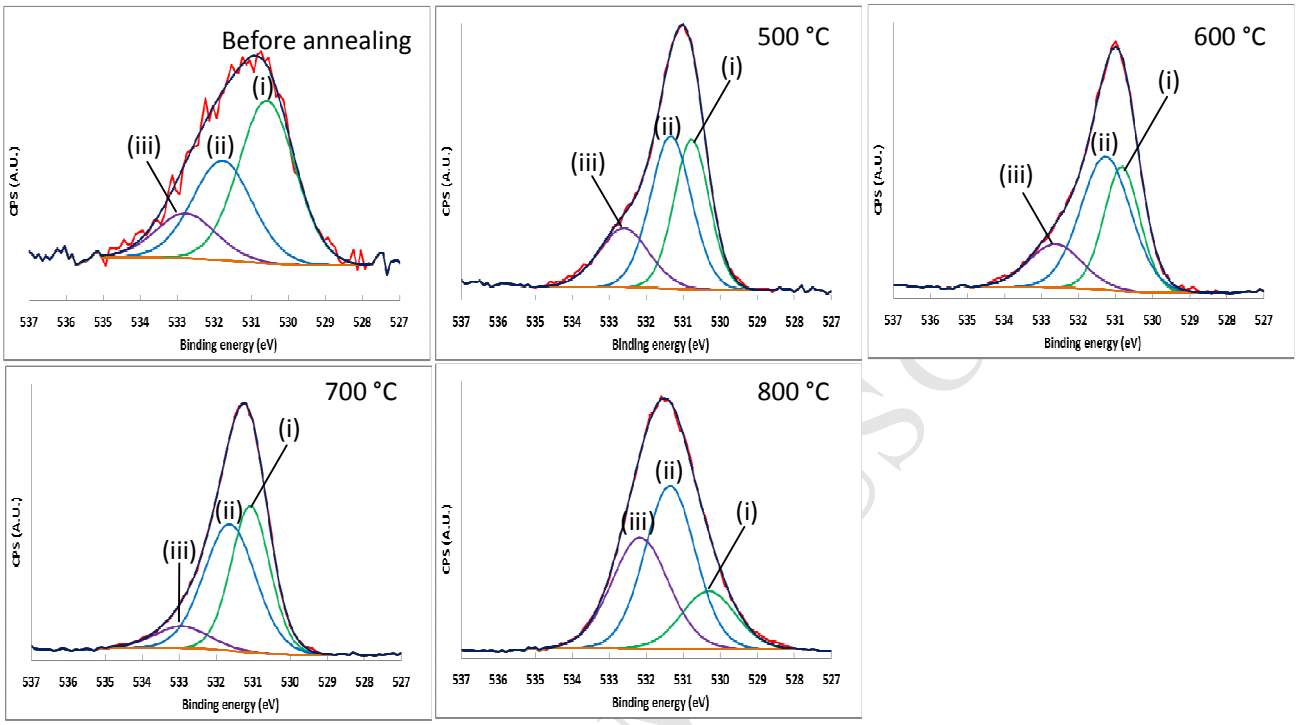

Figure 8. Typical fitting curves of O1*s* XPS spectra of sputtered TiAlSiN coatings before annealing and after being annealed at various temperatures.

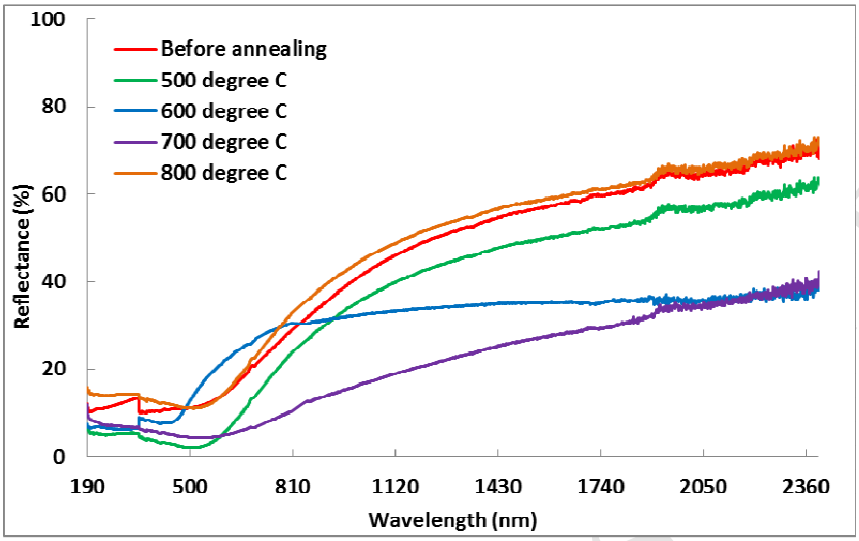

Figure 9. UV-Vis reflectance spectra of sputtered TiAlSiN coatings before annealing and after being annealed at 500-800 °C in steps of 100 °C.

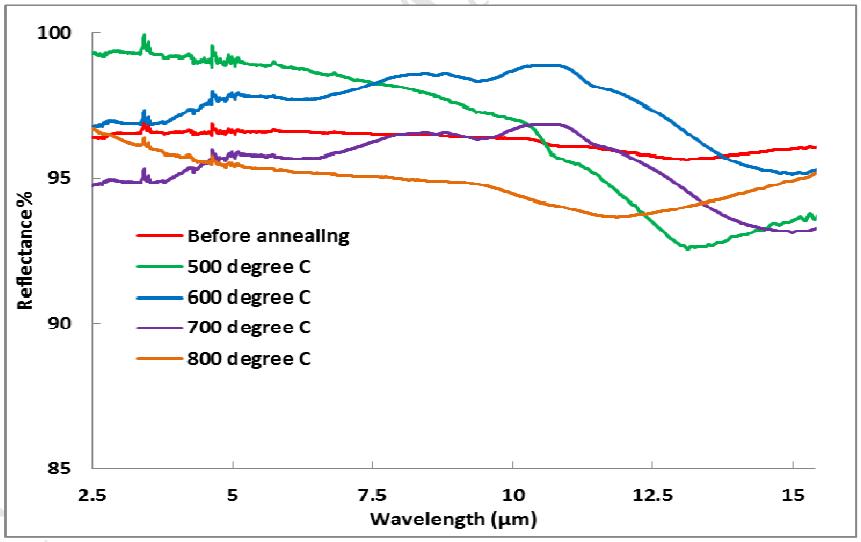

Figure 10. FTIR reflectance spectra of sputtered TiAlSiN coatings before annealing and after being annealed at 500-800 °C in steps of 100 °C.

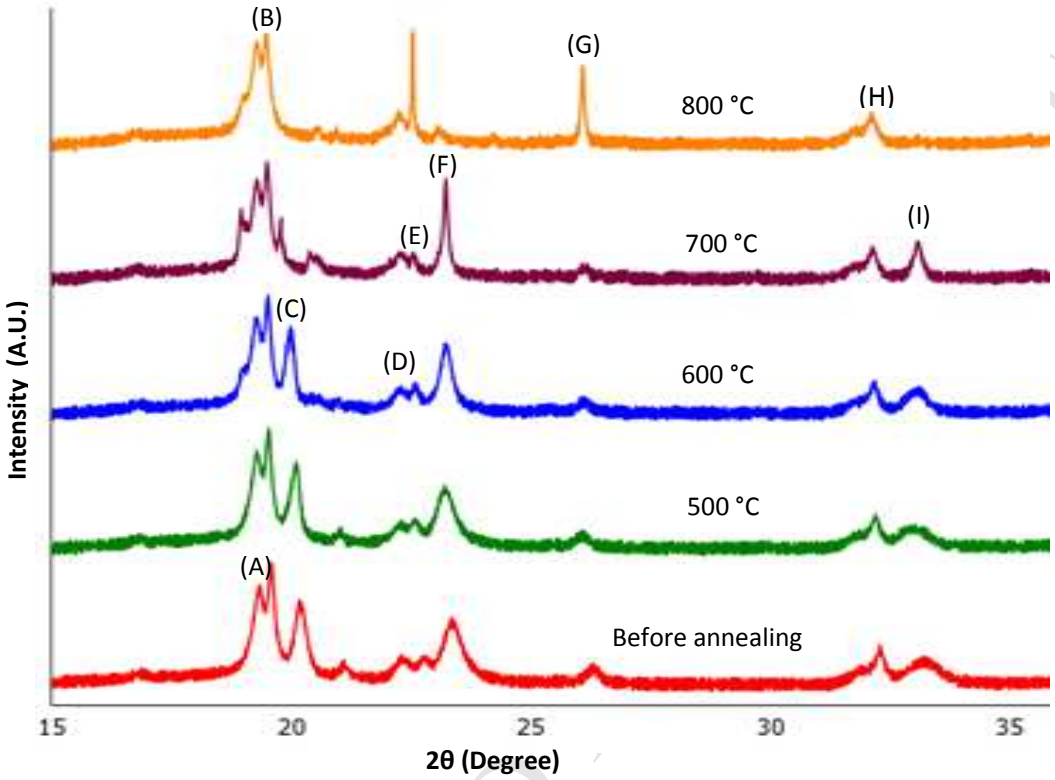

Figure 11. Synchrotron radiation X-ray diffraction (SR-XRD) data of sputtered TiAlSiN thin film coatings at different temperatures acquired in the powder diffraction beamline at Australian Synchrotron, Melbourne.

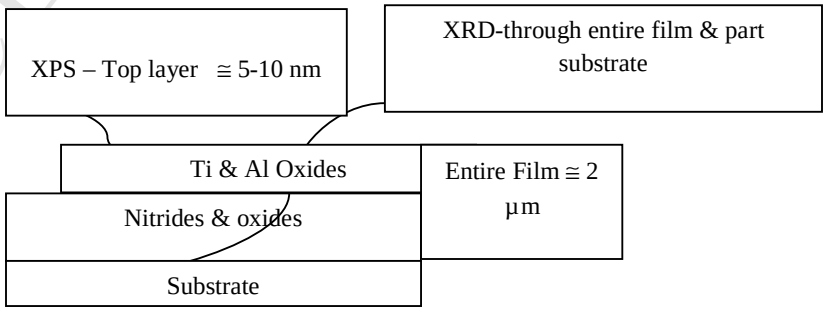

Figure 12. Schematic diagram of XPS and XRD penetration regions on samples at 800 °C. Also shown is the general type of phase compositions.

Highlights

- ✓ TiAlSiN sputtered coatings were characterized for solar selective applications
- ✓ In situ synchrotron radiation XRD were studies show the occurrence of multiple stable phases
- ✓ A high selectivity of 24.63 has been achieved for the coatings annealed at 700 ℃
- ✓ Existence of XRD phases were also confirmed by XPS measurements
- ✓ At high temperature annealing the mechanical properties of films were governed by the utmost surfaces of the films